PRELIMINARY RESULTS OF A STUDY OF THE RELATIONSHIP BETWEEN FREE-STREAM TURBULENCE AND STAGNATION REGION HEAT TRANSFER*

G. James VanFossen, Jr., and Robert J. Simoneau
National Aeronautics and Space Administration
Lewis Research Center
Cleveland, Ohio 44135

A study is being conducted at the NASA Lewis Research Center to investigate the mechanism that causes free-stream turbulence to increase heat transfer in the stagnation region of turbine vanes and blades. The work is being conducted in a wind tunnel at atmospheric conditions to facilitate measurements of turbulence and heat transfer. The model size is scaled up to simulate Reynolds numbers (based on the leading-edge diameter) that are to be expected on a turbine blade leading edge. Reynolds numbers from 13 000 to 177 000 were run in the present tests.

Spanwise-averaged heat transfer measurements with high and low turbulence have been made with "rough" and smooth surface stagnation regions. For smooth surfaces the boundary layer remained laminar even in the presence of free-stream turbulence. If roughness was added, the boundary layer became transitional as evidenced by the heat transfer increase with increasing distance from the stagnation line.

Hot-wire measurements near the stagnation region downstream of an array of parallel wires showed that vorticity in the form of mean velocity gradients was amplified as the flow approached the stagnation region. Circumferential traverses of a hot-wire probe near the surface of the cylinder showed that the fluctuating component of velocity changed in character depending on free-stream turbulence and Reynolds number.

Finally smoke-wire flow visualization and liquid-crystal surface heat transfer visualization were combined to show that, in the wake of an array of parallel wires, heat transfer was lowest where the fluctuating component of velocity (local turbulence) was highest. Heat transfer was the highest between pairs of vortices where the induced velocity was toward the cylinder surface.

SYMBOLS

D cylinder diameter, cm

d rod diameter, cm

e height of roughness element, cm

h heat transfer coefficient, W/m^2 °C

---

*Also published as NASA Technical Memorandum 86884.

q" heat flux, W/m^2

Re Reynolds number

T temperature, K

X distance measured upstream from forward stagnation line, cm

z spanwise coordinate, cm

θ circumferential coordinate, deg

INTRODUCTION

In gas turbine blade design, predicting heat transfer in the stagnation region is critical because the heat flux is usually highest in this region. The heat transfer in the stagnation region can be predicted if the free-stream flow is laminar (ref. 1). In a gas turbine, flows are highly turbulent, with intensities of 8 to 15 percent. If the turbulence intensity in the free stream is higher than 1 percent, heat transfer in the stagnation region is augmented.

Flow in the stagnation region of a turbine blade can be simulated by a cylinder in crossflow. There have been many experimental investigations of the effect of turbulence intensity on heat transfer to a cylinder in crossflow (e.g., refs. 2 to 6). Most of these investigations have measured an increase in heat transfer in the stagnation region for some increased level of free-stream turbulence and then tried to correlate the heat transfer increase to some parameter involving the turbulence intensity. This approach has had limited success. Trends are clearly present, but there is great scatter in the data, particularly between the data of different researchers.

The mathematical modeling of stagnation region flow has been divided into several areas. One set of modelers has attempted to develop a turbulence model that can be used to solve the two-dimensional boundary-layer equations and predict the level of heat transfer (refs. 2, 7, and 8). The results are a correlation of the mixing length or turbulent viscosity and the Prandtl number with other flow parameters.

A more plausible model of heat transfer augmentation by free-stream turbulence is the vortex stretching model. It is hypothesized that, as vortical filaments with components of their axes normal to the stagnation line and normal to the free-stream flow are convected into the stagnation region, they are stretched and tilted by the divergence of streamlines and acceleration around the body. Through conservation of angular momentum this stretching intensifies the vorticity. The increased vorticity is hypothesized to be the cause of the augmented heat transfer in the stagnation region. Some examples of the work on this theory are given in references 9 to 14, and the work is reviewed in reference 15. It was deduced (refs. 9 and 10) that the mathematical model allowed only turbulent eddies above a certain neutral scale to enter the Hiemenz flow (ref. 16) boundary layer. Once inside the boundary layer, however, the eddies can be broken down into smaller eddies by the action of viscosity. The three-dimensional vorticity transport equations were

solved for a free-stream velocity that was periodic in the spanwise coordinate. This boundary condition supplied the vorticity to the stagnation region in an orientation that allowed it to be stretched by the mean flow. A few special cases where the period in velocity was near the neutral scale have been solved. It was found that the thermal boundary layer is much more sensitive to external vorticity than the hydrodynamic boundary layer.

In reference 11 measurements of grid turbulence that contained eddies of all orientations near the stagnation point of a circular cylinder show that eddies with scales much larger than the cylinder diameter are not amplified as they approach the stagnation point but smaller scale eddies are amplified as they approach the cylinder. These measurements are external to the boundary layer. In references 12 and 13 a hot wire was used to measure the amplification of turbulence near the stagnation point of both a cylinder and an airfoil. The turbulence was produced by an upstream array of parallel rods. Spectral measurements were then used to deduce a so-called most-amplified scale. Flow visualization with smoke also shows a regular array of vortex pairs near the stagnation point. The array of vortex pairs is clearly outside the theoretical laminar boundary layer.

Reference 14 describes a threshold for vortex formation near the stagnation region of a bluff body from the wakes of an array of parallel wires placed upstream. If the wires are too far upstream or the Reynolds number is too small, no vortices are formed on a bluff body. Heat transfer augmentation in the stagnation region increases sharply when vortices are formed. The size of the vortices scales with the width of the upstream disturbance wake and not with boundary-layer thickness.

Calculations and measurements made in reference 5 show the boundary-layer velocity profiles to be essentially laminar even in the presence of free-stream turbulence. The temperature field, however, is more sensitive to free-stream turbulence. This implies that heat transfer will be increased more than skin friction by free-stream turbulence.

A collection of experimental observations has been assembled here to construct a picture of this complex phenomenon. Spanwise-averaged heat transfer data are presented to show the effect of free-stream turbulence and surface roughness on the condition (laminar or turbulent) of the thermal boundary layer. Hot-wire measurements are used to show how vorticity from mean velocity gradients is amplified as it approaches the stagnation region. Finally a combination of flow visualization using the smoke-wire technique and thermal visualization using liquid crystals is used to show the relationship between vortex pairs produced by mean velocity gradients and the spanwise heat transfer distribution.

APPARATUS

Wind Tunnel

All tests were conducted in the wind tunnel shown schematically in figure 1. Room air first flowed through a turbulence damping screen with an 18x18 mesh of 0.24-mm (0.0095-in) diameter wire. Large-scale turbulence from the room air was then broken up by flowing it through a honeycomb of approximately 12 000 plastic "soda straws," which were 0.64 cm (0.25 in) in

diameter by 19.69 cm (7.75 in) long. The air then passed through a final damping screen identical to the first. A 4.85:1 contraction (contraction in spanwise direction only) then accelerated the air entering the test section. The maximum velocity attainable in the test section was about 46 m/sec (150 ft/sec), and the clear-tunnel turbulence level was less than 0.5 percent at all flow rates.

The test section was 15.2 cm (6.0 in) wide by 68.6 cm (27.0 in) high. The models were mounted horizontally in the tunnel. Hot-wire surveys and smoke-wire flow visualization indicated that the center 7.6 cm (3.0 in) of the tunnel was free from turbulence generated by the side-wall boundary layer. All measurements were confined to this center region of the tunnel test section.

After leaving the test section the flow passed through a transition section into a 25-cm (10-in) pipe, through two long-radius elbows, into a flow straightener, and into an orifice run. The orifice plate had a diameter of 19.1 cm (7.5 in). The flow rates used in these tests were measured with this orifice. Air then passed through a 25-cm (10-in) butterfly valve, which was used to control the flow rate, and then to the building altitude exhaust system.

The temperature of the air entering the wind tunnel was measured by four exposed ball Chromel-Alumel thermocouples around the perimeter of the inlet. These four temperatures were averaged to give the total (or stagnation) temperature.

Turbulence Generators

For some of the high-turbulence cases a turbulence-generating biplane grid of 0.318-cm (0.125-in) diameter rods spaced 10 rod diameters apart was installed 79.6 rod diameters upstream of the model leading edge. For the flow visualization tests and some of the heat transfer tests an array of parallel 0.051-cm (0.020-in) diameter wires spaced 12.5 wire diameters apart was installed 547.5 wire diameters (4.21 cylinder diameters) upstream of the model leading edge. For the spanwise hot-wire traverses the same parallel-wire array was used, but the wires were spaced 37.5 wire diameters apart.

Hot Wire

Turbulence was measured with a constant-temperature, hot-wire anemometer. Signals were linearized, and the mean component of velocity was read on an integrating digital voltmeter with an adjustable time constant. The fluctuating component was read on a true rms voltmeter that also had an adjustable time constant. The hot-wire probe was a 4-μm (1.65-μin) diameter, tungsten, single-wire probe. The hot wire was calibrated before each use in a free jet of air at nearly the same temperature ($\pm$1 deg C) as the wind tunnel flow. The frequency response of the hot-wire system was determined to be around 30 kHz by the standard square-wave test.

Turbulence scale was estimated by using an autocorrelation of the hot-wire signal. The autocorrelation was obtained on a dual-channel, fast Fourier transform (FFT) spectrum analyzer. The area under the autocorrelation

function gave an integral time scale. This time scale was then multiplied by the mean velocity to obtain the integral length scale.

Smoke Wire

Flow visualization was accomplished by using the smoke-wire technique described in reference 17. A 0.008-cm (0.003-in) diameter wire was stretched across the tunnel parallel to the cylinder axis slightly below the stagnation plane. The wire was coated with oil, as recommended in reference 17, by using a cotton swab. A timing circuit was then used to start current flow to heat the wire and vaporize the oil and, after an adjustable delay, to fire a strobe light to expose the film. A 35-mm camera with telephoto lens and closeup attachments was then used to make high-quality images of the flow and heat transfer patterns in the stagnation region. Two strobe lights were used, one from each side of the tunnel. The best lighting angle for smoke visualization was 90° from the viewing angle. This angle was not an optimum angle for the viewing of the liquid-crystal models. As explained in reference 18, if the lighting angle and the viewing angle are not the same, there is a color shift in the liquid crystal. Thus simultaneous smoke and liquid-crystal thermal visualization photographs can only be used to obtain qualitative heat transfer results.

TEST SPECIMENS

Spanwise-Averaged Heat Transfer

Spanwise-averaged heat transfer coefficients were measured on a 6.6-cm (2.6-in) diameter cylinder (fig. 2). The cylinder was 15.2 cm (6 in) long and was made of wood. Heat transfer coefficients around the circumference of the cylinder were measured with electrically heated copper strips (fig. 3). Each strip was 6.6 cm (2.6 in) long by 0.51 cm (0.21 in) wide and 0.318 cm (0.125 in) deep. A Kapton-encapsulated electric heater was fastened to the back of each copper strip with pressure-sensitive adhesive. A stainless steel sheathed, closed, grounded-ball, Chromel-Alumel thermocouple was soft soldered into a groove in each copper strip. The copper heat flux gauges were embedded in the surface of the cylinder at 10° intervals around the circumference. The average gap between copper strips was 0.10 cm (0.04 in) and was filled with epoxy. Although there were eight copper strips, only the inner six strips were used as measuring gauges; the outer two served as guard heaters to minimize heat loss by conduction. Guard heaters were also used on the ends of the copper strip gauges (fig. 2). A guard heater was also used behind the measuring gauges to stop radial heat conduction to the rear of the cylinder. A thin coat of lacquer was sprayed on the surface of the cylinder and the copper gauges to keep the copper from oxidizing and changing emissivity. In operation the copper strips were maintained at a constant temperature by a controller described in reference 19. The data reduction technique used for the spanwise-averaged model is also described in reference 19.

For some of the tests, the spanwise-averaged heat transfer model was used to investigate the effect of surface roughness. A coat of clear lacquer was sprayed onto the model, and sand was then sprinkled on the wet surface from an ordinary salt shaker. Another thin coat of lacquer then held the sand in place. Since the roughness elements were too large to be measured with a

profilometer, an optical comparator was used to estimate roughness. The maximum height of any one roughness element was 0.0572 cm (0.0225 in). The average height of the roughness elements above the surface was 0.033 cm (0.013 in), which gave a relative roughness e/D of 0.005.

An afterbody was used with the cylinder for some tests to eliminate the alternate vortex shedding from the rear of the cylinder. The afterbody consisted of a 5.08-cm (2.0-in) long straight segment that was tangent to the cylinder surface 90° from the stagnation line. A 10° wedge then extended downstream and ended in a cylindrical trailing edge 0.3175 cm (0.125 in) in diameter.

Liquid-Crystal Models

Spanwise variations in heat transfer coefficient were mapped with three models (fig. 4). One was a cylinder with the same dimensions as the spanwise-averaged heat transfer model. The second had the same dimensions as the spanwise-averaged model plus the afterbody. The third was scaled to one-half the size of the spanwise-averaged model plus the afterbody.

All of the liquid-crystal models were constructed by using the techniques in reference 18. Briefly, a heater element consisting of polyester sheet with a vapor-deposited gold layer was fastened to the model surface with double-sided tape. Bus bars of copper foil were fastened to the heater edges, which were parallel to the cylinder axis and located at the rear of the cylinder. Silver conductive paint was used to improve electrical conductance between the copper foil and the gold. A commercially available plastic sheet containing cholesteric liquid crystals was fastened over the heater with double-sided tape.

The gold heater was checked for uniformity in still air by using the liquid-crystal sheets to monitor temperature gradients. The liquid crystal was calibrated in a water bath to determine the temperature that corresponded to color. Yellow indicated a temperature of 54.8 $\pm$ 0.2 °C (130.6 $\pm$ 0.4 °F).

In operation, the cylinder was heated by passing an electric current through the gold film. This supplied a uniform heat flux at the surface of the cylinder. Electric power to the model was adjusted so that the area of interest on the surface turned yellow. Neglecting radiation and conduction losses, which are small, the heat transfer coefficient can be computed as

$$h = \frac{q''}{T_{yellow} - T_{air}}$$

Thus yellow traces an iso-heat-transfer coefficient contour on the model.

Traversing Cylinder

Turbulence measurements near the surface of the cylinder were made with a traversing cylinder (fig. 5). This cylinder was made of wood and had a hole drilled along a diameter. A hot-wire probe could be inserted through this hole and positioned close to the surface. The area around the hot-wire probe

was filled in with modeling clay to match the contour of the cylinder. The traversing cylinder extended through holes in the tunnel walls; felt was used as a seal between the cylinder and the walls. The cylinder could thus be traversed axially across the tunnel span or rotated about its axis, carrying the hot wire with it.

ERROR ANALYSIS

An error analysis was performed for each of the spanwise-averaged heat transfer data points by the method of Kline and McClintock (ref. 20). The average error for all of the data points was 5.7 percent, and the maximum error for any one data point was 7.8 percent. Error estimates were not made for the hot-wire and liquid-crystal data.

RESULTS AND DISCUSSION

In this section spanwise-averaged heat transfer distributions around a circular cylinder in cross flow, are presented for high and low free-stream turbulence as well as the effect of surface roughness. Hot-wire measurements are presented to demonstrate amplification of vorticity in the free stream as the flow approaches the stagnation region. Finally, flow visualization and thermal visualization are combined to show the relationship between vortex pairs formed in the stagnation region and spanwise variations in surface heat transfer.

Spanwise-Averaged Heat Transfer

Nusselt number as a function of angle from the stagnation point was determined for the four cases (fig. 6). All of the data were taken at a Reynolds number of 177 000 (based on free-stream conditions and cylinder diameter). Low-turbulence data were taken with a clear tunnel and high-turbulence data were taken with a biplane grid. The grid produced turbulence of about 2.4 percent with a scale of 0.50 cm (0.20 in). Also plotted on the figure is an exact solution of the laminar boundary-layer equations due to reference 1. The data shown on figure 6 were for the cylinder without the afterbody; data taken with the afterbody in place were identical within experimental error.

Smooth surface - low turbulence. - The agreement between the exact solution and the smooth-cylinder, low-turbulence data is well within the experimental error and thus confirms the accuracy of the experimental method (fig. 6).

Smooth surface - high turbulence. - For the cylinder placed downstream of the biplane grid (fig. 6) turbulence increased the heat transfer virtually uniformly around the circumference (measurements were only made up to 50° from stagnation) by about 30 percent. This agrees well with the data of other observers: for example, the theory of reference 2 predicts an increase in Nusselt number at the stagnation point of 27.8 percent for these conditions.

Rough surface - low turbulence. - Adding sand roughness to the cylinder surface with 0.5-percent free-stream turbulence did not change the heat

transfer rate at the stagnation point from the smooth-surface case (fig. 6). As the angle from stagnation increased, however, the heat transfer rate also increased, most likely because boundary-layer transition was triggered by the roughness elements.

Rough surface - high turbulence. - For the sand-roughened surface with 2.4-percent free-stream turbulence the effect of free-stream turbulence was greatest nearest the stagnation point, where the heat transfer rate was again about 30 percent higher than in the low-turbulence case. As the angle from stagnation became larger, the high- and low-turbulence data (rough surface) merged as the boundary layer became more turbulent.

Surface roughness had no effect on heat transfer at the stagnation line but changed the character of the boundary layer in the downstream direction. It seems that the boundary layer on the smooth surface remains laminar at the Reynolds numbers tested (i.e., no turbulence is produced within the boundary layer). Free-stream turbulence somehow acts on a laminar boundary layer to augment heat transfer.

Hot-Wire Measurements

Streamwise traverse. - A streamwise traverse of a single hot wire was performed with the wire oriented parallel to the 6.6-cm (2.6-in) diameter cylinder axis and as close as possible to the plane of the stagnation streamline. An array of 0.05-cm (0.02-in) parallel wires spaced 12.5 wire diameters apart was located 4.21 cylinder diameters (547.5 wire diameters) upstream of the stagnation point. This wire array produced vorticity (gradients in the mean velocity) in an orientation that could be stretched and amplified. The traverse was made 0.044 to 3.06 cylinder diameters upstream of the stagnation point at a Reynolds number of 177 000 (based on cylinder diameter). It is typical of all traverses made over the Reynolds number range (31 000 to 177 000). The mean velocity (fig. 7) fell monotonically as the stagnation region was approached. The fluctuating velocity (rms, fig. 7), however, first decayed with distance downstream of the grid (decreasing X/D) and then sharply increased and peaked at about 0.085 cylinder diameter upstream from the stagnation point. This peak was far outside the predicted laminar boundary-layer thickness of 0.003 cylinder diameter (ref. 16). These results are very similar to those of reference 12.

Spanwise traverse. - Two spanwise traverses of a hot wire oriented perpendicular to the cylinder axis and centered in the plane of the stagnation streamline were made. The cylinder leading edge was located 4.21 cylinder diameters downstream of an array of 0.05-cm (0.02-in) diameter parallel wires spaced 37.5 wire diameters apart. Both traverses were made at a Reynolds number of 31 000 (based on cylinder diameter) and are typical of those for the complete Reynolds number range. Both traverses are presented at the same scale in figure 8. For the traverse taken at 1.06 cylinder diameters upstream from the stagnation line, the wire wakes are clearly visible in the mean velocity trace. The turbulent fluctuations are high in the wire wakes and low in the relatively undisturbed flow between wires. At 0.095 cylinder diameter upstream the mean velocity greatly decreased, but the depth of the wake increased, an indication of increasing vorticity as the stagnation region was approached. The fluctuating component of velocity also increased in the wire wakes as the stagnation region was approached.

Circumferential traverses. - A hot wire oriented parallel to the cylinder axis and located 0.012 cylinder diameter from the cylinder surface was traversed in the circumferential direction $\pm 21°$ at a Reynolds number of 125 000 (based on cylinder diameter). For the clear tunnel (fig. 9(a); i.e., free-stream turbulence intensity less than 0.5 percent), the mean velocity increased with angle from stagnation as the flow accelerated around the body, and the fluctuating component of velocity was lowest at the stagnation point. This functional form of the fluctuating velocity with angle was independent of Reynolds number for all flows tested with the clear tunnel. For an array of parallel 0.05-cm (0.02-in) diameter wires spaced 12.5 wire diameters apart and located 547.5 wire diameters upstream of the stagnation line (fig. 9(b)), the mean velocity trace was identical to that for the clear tunnel, but the fluctuating velocity had completely changed. The minimum at the stagnation line in the clear tunnel changed to a maximum, and the level away from the stagnation region decreased. The large variations in fluctuating velocity with angle in the clear tunnel were damped. This change in character was Reynold-number dependent: below a Reynolds number of 95 000 (based on cylinder diameter; 730 based on wire diameter), the fluctuating velocity was at a minimum at the stagnation point with or without a wire array (fig. 9(a)). Above a Reynolds number of 95 000 the fluctuating velocity looked like figure 9(b). We have no explanation for this phenomenon.

Simultaneous Flow - Thermal Visualization

The smoke-wire flow visualization and liquid-crystal thermal visualization techniques were combined to show the relationship between spanwise variations in heat transfer and vortices in the stagnation region. These vortices were formed from the wakes of wires placed upstream of the cylindrical leading edge and arranged as shown in figure 5. The leading-edge region for the 6.6-cm (2.6-in) diameter cylindrical-leading-edge model with afterbody taken at a Reynolds number of 13 000 is shown in figure 10. The Reynolds number for the wires was about 100; for wire Reynolds numbers less than 120 the wakes were laminar (i.e., no Karman trails were formed). The dark lines on the surface of the model were drawn in a 1.27-cm (0.5-in) square grid pattern for visual scaling. The model and relative camera position are shown in figure 11.

The smoke shows that a vortex pair formed from the wake of each wire. The vortices were well outside the theoretical laminar boundary layer. The dark, vertical stripes in the liquid crystal were regions of low temperature and thus high heat transfer. Thus, contrary to expectations, the regions of highest heat transfer were not under the vortices but between vortex pairs, where the free-stream turbulence was lowest. In this region the induced velocity from neighboring vortex pairs was directed toward the cylinder surface. Conversely, the region of minimum heat transfer was directly under the vortex pair. This was the region of highest free-stream turbulence as measured by a hot wire outside the boundary layer. Figure 12 shows schematically the spatial relationship of the wires, wakes, vortex pairs, and the peaks in heat transfer.

The heat transfer - vortex pattern was the same for all three models used (fig. 4). It was the same for the cylinder without the afterbody as for cylinder with the afterbody. The half-scale model with the afterbody also had the same heat transfer pattern, but the vortices appeared smaller in diameter

at the same free-stream velocity. The spanwise spacing of vortex pairs remained equal to the wire spacing. The Reynolds number for the half-scale model was one-half that for the large cylinder with the afterbody.

For the half-scale model the spanwise heat transfer coefficient varied along the stagnation line (i.e., (maximum h - minimum h)/0.5 (maximum h + minimum h)) from 7 percent at a Reynolds number of 16 000 to 16 percent at a Reynolds number of 89 000. This is the magnitude found for spanwise variations in mass transfer caused by periodic irregularities in a screen (ref. 21). Such measurements were not made for the other models.

High-speed motion pictures of smoke near the stagnation point of the cylinder without the afterbody were taken at a Reynolds number of 13 000. Vortices still were formed in the stagnation region, but the stagnation point oscillated because of alternate vortex shedding from the rear of the cylinder.

Vortices were only visible for Reynolds numbers less than about 120 (based on wire diameter). At higher Reynolds numbers the wire wakes became unstable and finally fully turbulent, making it impossible to see the vortices. The heat transfer pattern, however, remained unchanged at all Reynolds numbers, indicating that the vortices must still be there although they could not be seen. A time-exposure photograph was taken in the hope that the random fluctuations from the wire wakes would be averaged out and the relatively steady vortex pattern would thus be made visible. The random fluctuations were indeed averaged out, but no steady vortices could be seen.

SUMMARY OF RESULTS

This report has presented preliminary results of a study to investigate the relationship between free-stream turbulence and heat transfer augmentation in the stagnation region. The effects of free-stream turbulence and surface roughness on spanwise-averaged heat transfer were investigated. Turbulence was measured upstream of a cylinder placed in the wake of an array of parallel wires that were perpendicular to the cylinder axis. Finally, flow visualization and thermal visualization techniques were combined to show the relationship between vortices in the stagnation region and spanwise variations in heat transfer.

The major conclusions were as follows:

1. Surface roughness has no effect on heat transfer at the stagnation point.

2. Free-stream turbulence has the same effect on heat transfer at the stagnation point for smooth and rough cylinders.

3. The boundary layer downstream of the stagnation point remains laminar in the presence of free-stream turbulence and is forced into transition by surface roughness for the range of Reynolds numbers and turbulence levels tested.

4. Vorticity in the form of mean velocity gradients is amplified as it approaches the stagnation region.

5. Turbulent fluctuating velocity is amplified as it approaches the stagnation region, reaches a peak, and then is damped as it approaches the boundary layer.

6. Heat transfer in the stagnation region is highest where the turbulent fluctuations are lowest. This occurs between the wakes formed by parallel wires upstream and perpendicular to the axis of the cylinder. This corresponds to the region between vortex pairs, where the velocity induced by the vortices is toward the cylinder surface. Conversely, the lowest heat transfer occurs where the induced velocity is away from the cylinder surface.

7. Vortices formed in the stagnation region from mean velocity gradients are well outside the theoretical laminar boundary layer.

REFERENCES

1. Frossling, N., "Evaporation, Heat Transfer, and Velocity Distribution in Two-Dimensional and Rotationally Symmetrical Laminar Boundary-Layer Flow," NACA TM-1432, 1958.

2. Smith, M.C., and Kuethe, A.M., "Effects of Turbulence on Laminar Skin Friction and Heat Transfer," Physics of Fluids, Vol. 9, No. 12, Dec. 1966, pp. 2337-2344.

3. Kestin, J., and Wood, R.T., "The Influence of Turbulence on Mass Transfer from Cylinders," Journal of Heat Transfer, Vol. 93, No. 11, Nov. 1971, pp. 321-327.

4. Giedt, W.H., "Effect of Turbulence Level of Incident Air Stream on Local Heat Transfer and Skin Friction on a Cylinder," Journal of the Aeronautical Sciences," Vol. 18, No. 11, Nov. 1951, pp. 725-730, 766.

5. Hanarp, L.R., and Sunden, B.A., "Structure of the Boundary Layers on a Circular Cylinder in the Presence of Free Stream Turbulence," Letters in Heat and Mass Transfer, Vol. 9, May-June 1982, pp. 169-177.

6. Lowery, G.W., and Vachon, R.I., "Effect of Turbulence on Heat Transfer from Heated Cylinders," International Journal of Heat and Mass Transfer, Vol. 18, No. 11, Nov. pp. 1229-1242.

7. Wang, C.R., "Turbulence and Surface Heat Transfer Near the Stagnation Point of a Circular Cylinder in Turbulent Flow," NASA TM-83732, 1984.

8. Gorla, R.S.R., and Nemeth, N., "Effects of Free Stream Turbulence Intensity and Integral Length Scale on Heat Transfer From a Circular Cylinder in Crossflow," U. Grigull, et al., eds., Heat Transfer 1982, Vol. 3, Hemisphere Publishing Corp., Washington, D.C., 1982, pp. 153-158.

9. Sutera, S.P., Maeder, P.F., and Kestin, J., "On the Sensitivity of Heat Transfer in the Stagnation-Point Boundary Layer to Free-Stream Vorticity," Journal of Fluid Mechanics, Vol. 16, Part 4, Aug. 1963, pp. 497-520.

10. Sutera, S.P., "Vorticity Amplication in Stagnation-Point Flow and Its Effect on Heat Transfer, Journal of Fluid Mechanics, Vol. 21, Part 3, Mar. 1965, pp. 513-534.

11. Britter, R.E., Hunt, J.C.R., and Mumford, J. C., "The Distortion of Turbulence by a Circular Cylinder," Journal of Fluid Mechanics, Vol. 92, Part 2, May 28, 1979, pp. 269-301.

12. Sadeh, W.Z., and Brauer, H.J., "Coherent Substructure of Turbulence Near the Stagnation Zone of a Bluff Body," Journal of Wind Engineering and Industrial Aerodynamics, Vol. 8, No. 1-2, July 1981, pp. 59-72.

13. Sadeh, W.Z., and Sullivan, P.P., "Turbulence Amplification in Flow About an Airfoil," ASME Paper 80-GT-111, Mar. 1980.

14. Hodson, P.R., and Nagib, H.M., "Vortices Induced in a Stagnation Region by Wakes-Their Incipient Formation and Effects on Heat Transfer from Cylinders," AIAA Paper 77-790, June 1977.

15. Morkovin, M.V., "On the Question of Instabilities Upstream of Cylindrical Bodies," NASA CR-3231, 1979.

16. Schlichting, H., "Boundary Layer Theory," 4th ed., McGraw Hill, p. 78.

17. Jansen, B.J. Jr., "Flow Visualization Through the Use of the Smoke Wire Technique," AIAA Paper 81-0412, Jan. 1981.

18. Hippensteele, S.A., Russell, L.M., and Stepka, F.S., "Evaluation of a Method for Heat Transfer Measurements and Thermal Visualization Using a Composite of a Heater Element and Liquid Crystals," Journal of Heat Transfer, Vol. 105, No. 1, Feb 1983, pp. 184-189.

19. VanFossen, G.J., et al., "Heat Transfer Distributions Around Nominal Ice Accretion Shapes Formed on a Cylinder in the NASA Lewis Icing Research Tunnel," AIAA Paper 84-0017, Jan. 1984.

20. Kline, S.J., and McClintock, F.A., "Describing Uncertainties in Single-Sample Experiments," Mechanical Engineering, Vol. 75, No. 1, Jan. 1953, pp. 3-8.

21. Marziale, M.L., and Mayle, R.E., "Mass Transfer From a Circular Cylinder-Effects of Flow Unsteadiness and 'Slight Nonuniformities'," Rensselaer Polytechnic Institute, Troy, New York, Sept. 1984. (NASA CR-174759).

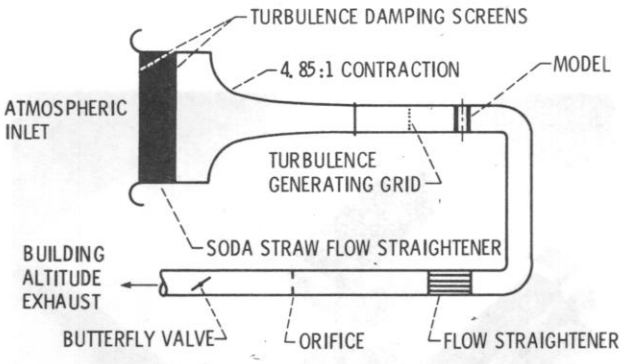

Figure 1. - Schematic of wind tunnel.

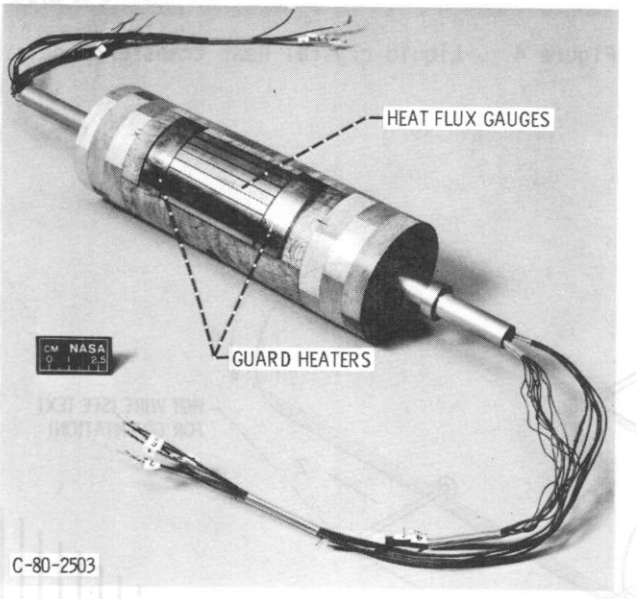

Figure 2. - Spanwise-averaged heat transfer model.

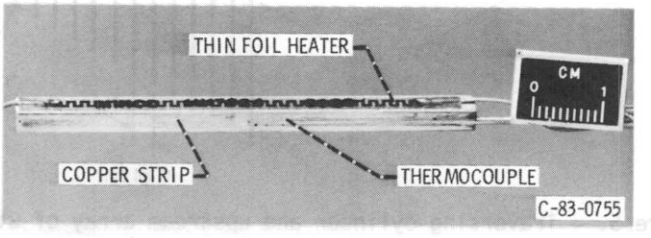

Figure 3. - Heat flux gauge.

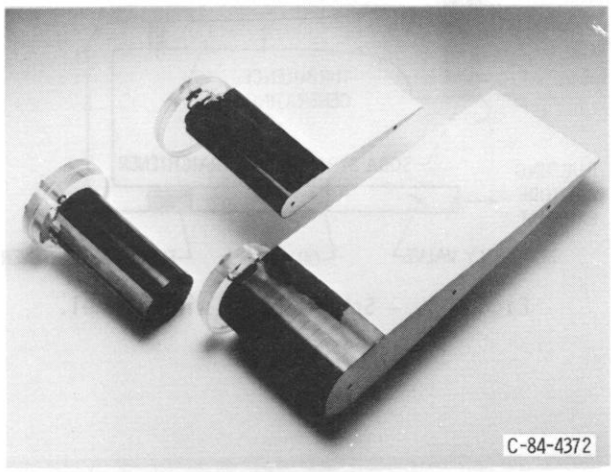

Figure 4. - Liquid-crystal heat transfer models.

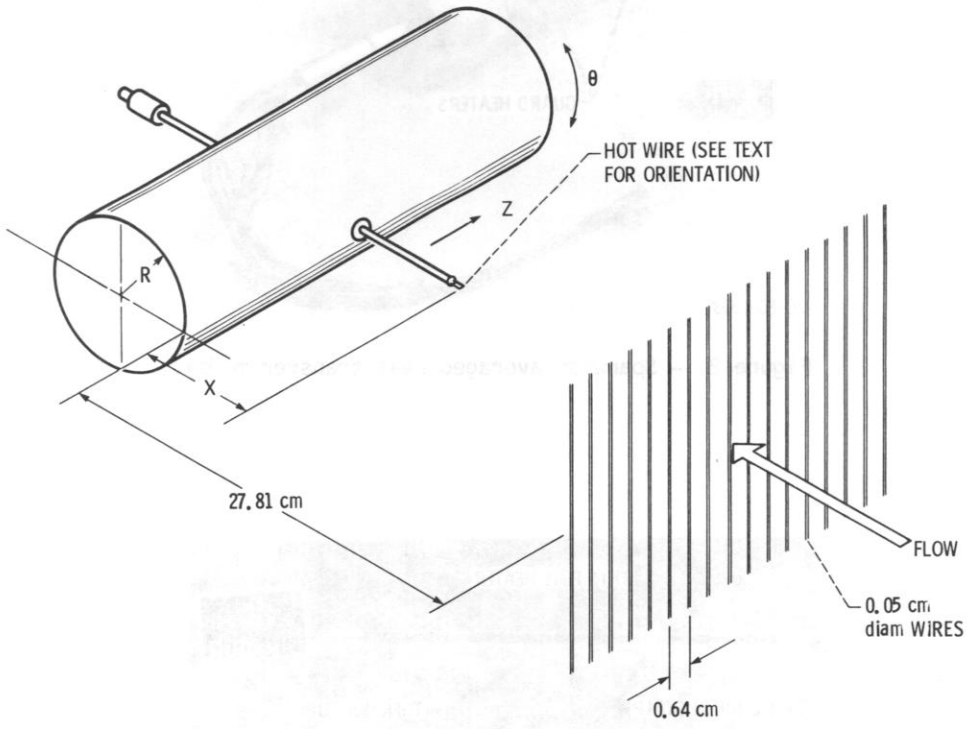

Figure 5. - Traversing cylinder and upstream array of wires.

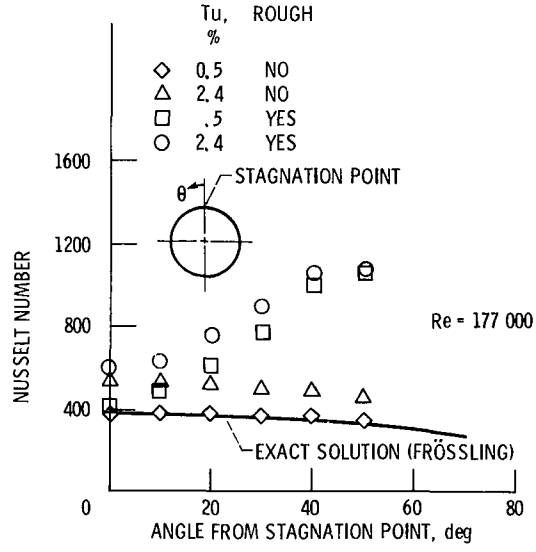

Figure 6. - Effect of free-stream turbulence and surface roughness on spanwise-averaged heat transfer for cylinder in crossflow. Re = 177 000.

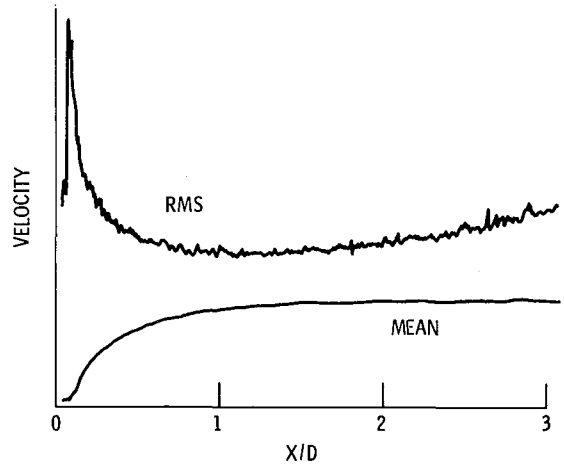

Figure 7. - Streamwise traverse of hot wire close to stagnation streamline.

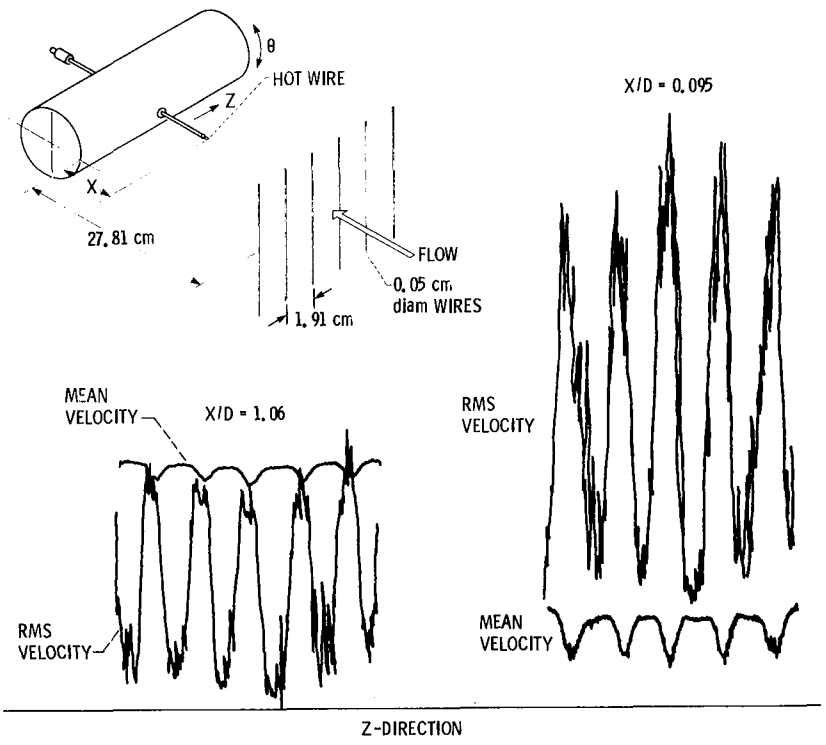

Figure 8. - Spanwise traverses of hot wire near cylinder stagnation point. (Abscissa of rms and mean velocity plots is offset slightly because of pen offset on x-yy' recorder.)

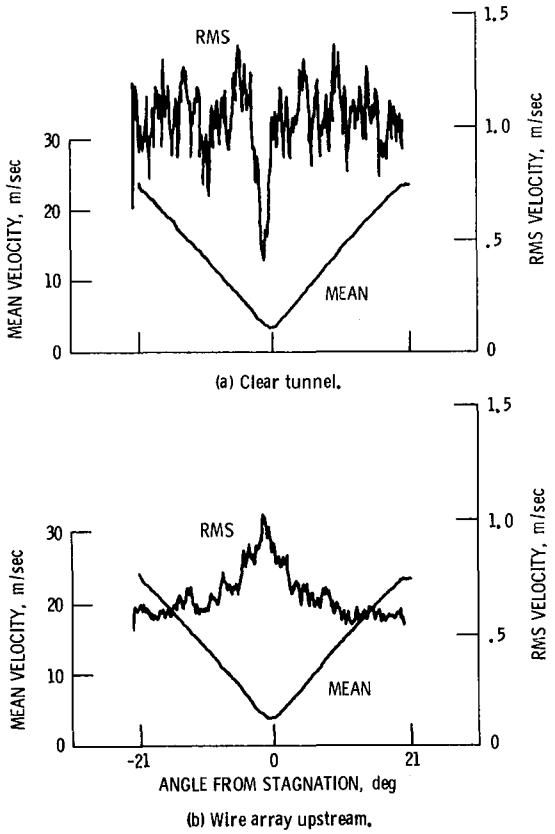

Figure 9. - θ-direction hot-wire traverse. Re_D = 125 000.

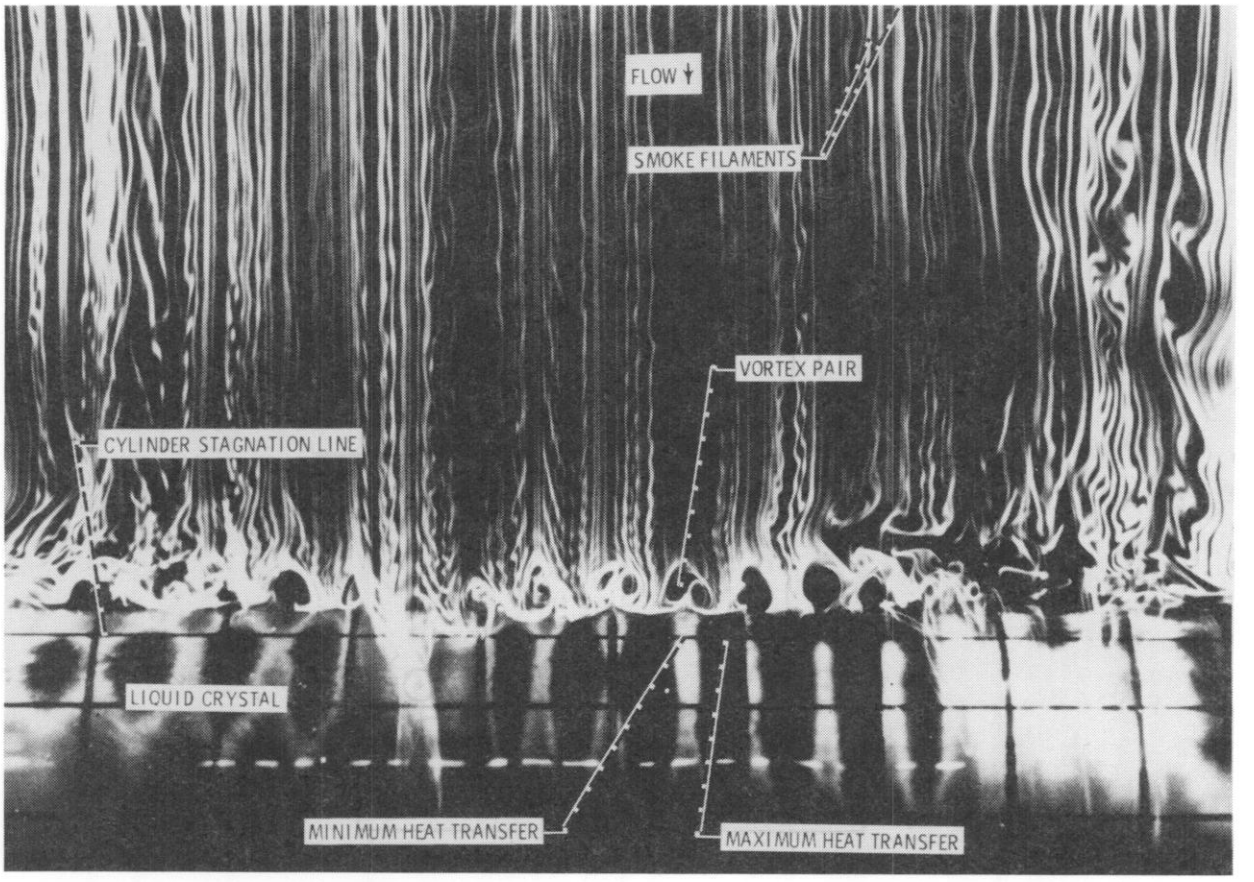

Figure 10. - Combined thermal and flow visualization of cylinder in crossflow.

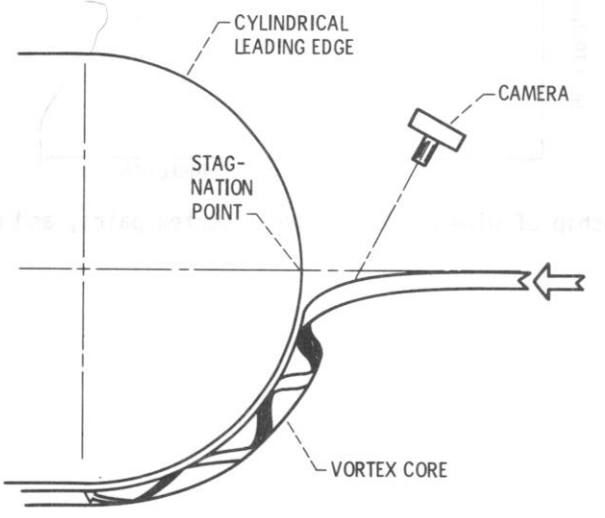

Figure 11. - Liquid-crystal model and relative camera position.

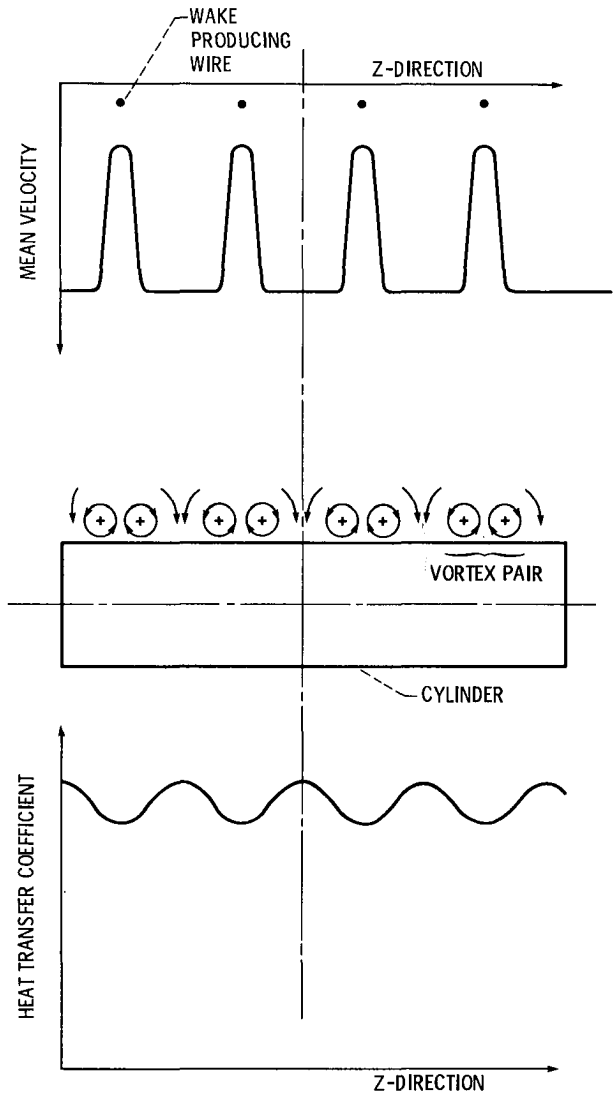

Figure 12. - Relationship of wire-produced wakes, vortex pairs, and peaks in heat transfer.